

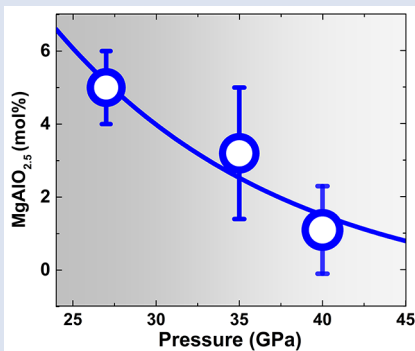
Rapid decrease of MgAlO_{2.5} component in bridgmanite with pressure

Z. Liu^{1*}, T. Ishii¹, T. Katsura¹



doi: 10.7185/geochemlet.1739

Abstract



The solubility of the MgAlO_{2.5} component in bridgmanite was measured at pressures of 27, 35 and 40 GPa and a temperature of 2000 °K using an ultra-high pressure multi-anvil press. Compositional analysis of recovered samples demonstrated that the MgAlO_{2.5} component decreases with increasing pressure, and approaches virtually zero at 40 GPa. Above this pressure, the MgAlO_{2.5} component, *i.e.* the oxygen-vacancy substitution, becomes negligible, and Al is incorporated in bridgmanite by the charge-coupled substitution only. These results are supported by the volume change associated with the change from the oxygen-vacancy substitution to charge-coupled substitution. The present result may explain the seismically observed slab stagnation in the mid-lower mantle. Although bridgmanite has been put forward as a potential host for water and argon in the lower mantle by trapping them in oxygen vacancies, such capabilities will rapidly decrease with depth and be lost in regions deeper than 1000 km.

Received 10 May 2017 | Accepted 8 September 2017 | Published 12 October 2017

Introduction

Aluminium (Al) is the fifth most abundant element in the Earth's mantle (McDonough and Sun, 1995). Under the Earth's lower mantle conditions, Al³⁺ is mainly accommodated in bridgmanite in a pyrolite mantle (Irifune, 1994). Al substitution in the Mg, Si or both sites modifies the crystal chemistry of bridgmanite, and thereby changes the physical properties of bridgmanite (Zhang and Weidner, 1999; Brodholt, 2000). Therefore, understanding the Al substitution mechanism is essential to investigating the mineralogy and dynamics of the lower mantle.

Two competing Al substitution mechanisms occur in bridgmanite (Hirsch and Shankland, 1991). One is the charge-coupled substitution ($\text{Mg}^{2+} + \text{Si}^{4+} = \text{Al}^{3+} + \text{Al}^{3+}$; components along the MgSiO₃–Al₂O₃ binary system), where two Al cations substitute for one Mg with the roughly 8-fold coordination (A site) and one Si with the 6-fold coordination (B site). The other mechanism is the oxygen-vacancy substitution ($2\text{Si}^{4+} + \text{O}^{2-} = 2\text{Al}^{3+} + \text{V}_\text{O}$, where V_O is an oxygen vacancy; components along the MgSiO₃–MgAlO_{2.5} binary system), where two Al cations replace two Si in the B sites and one oxygen vacancy forms to compensate for the excess negative charges. The oxygen vacancies in bridgmanite have special importance for understanding lower mantle processes because oxygen vacancies may induce water ($\text{V}_\text{O} + \text{O}^{2-} + \text{H}_2\text{O} = 2\text{OH}^{-1}$; Navrotsky, 1999) and noble gases into bridgmanite (Shcheka and Keppler, 2012).

Earlier theoretical calculations investigated whether oxygen vacancies exist in bridgmanite (Brodholt, 2000; Yamamoto *et al.*; 2003; Akber–Knutson and Bukowinski, 2004). Brodholt (2000) suggested that oxygen-vacancy substitution should dominate at pressures only up to 30 GPa. Yamamoto *et al.* (2003) argued oxygen-vacancy substitution should be unfavourable in the entire lower mantle. Furthermore, energetic calculations by Akber–Knutson and Bukowinski (2004) suggested that oxygen-vacancy substitution could only account for 3–4 % and less than 1 % of Al substitutions in the shallower and deeper parts of the lower mantle, respectively.

High pressure and high temperature synthesis (Navrotsky *et al.*, 2003) and nuclear magnetic resonance (NMR) spectroscopy (Stebbins *et al.*, 2003) suggested that oxygen-vacancy substitution dominates in bridgmanite with 5–10 mol. % MgAlO_{2.5} at 27 GPa and 1873 °K. On the other hand, X-ray diffraction measurements in a laser-heated diamond anvil demonstrated that bridgmanite coexisted with periclase from a glass starting material with a composition of 90 mol. % MgSiO₃ and 10 mol. % MgAlO_{2.5} at 40 ± 10 GPa and 2000–2500 °K (Walter *et al.*, 2006), indicating that the MgAlO_{2.5} component was not present in bridgmanite and thereby oxygen-vacancy substitution was unfavoured under these conditions. Note that pressure and temperature uncertainties in this study were relatively large, and the composition of bridgmanite was not determined owing to its very small sample size. Thus, it is still uncertain whether MgAlO_{2.5} can be a dominant component in bridgmanite in the lower mantle.

1. Bayerisches Geoinstitut, University of Bayreuth, 95440 Bayreuth, Germany
* Corresponding author (email: zhaodong.liu@uni-bayreuth.de)



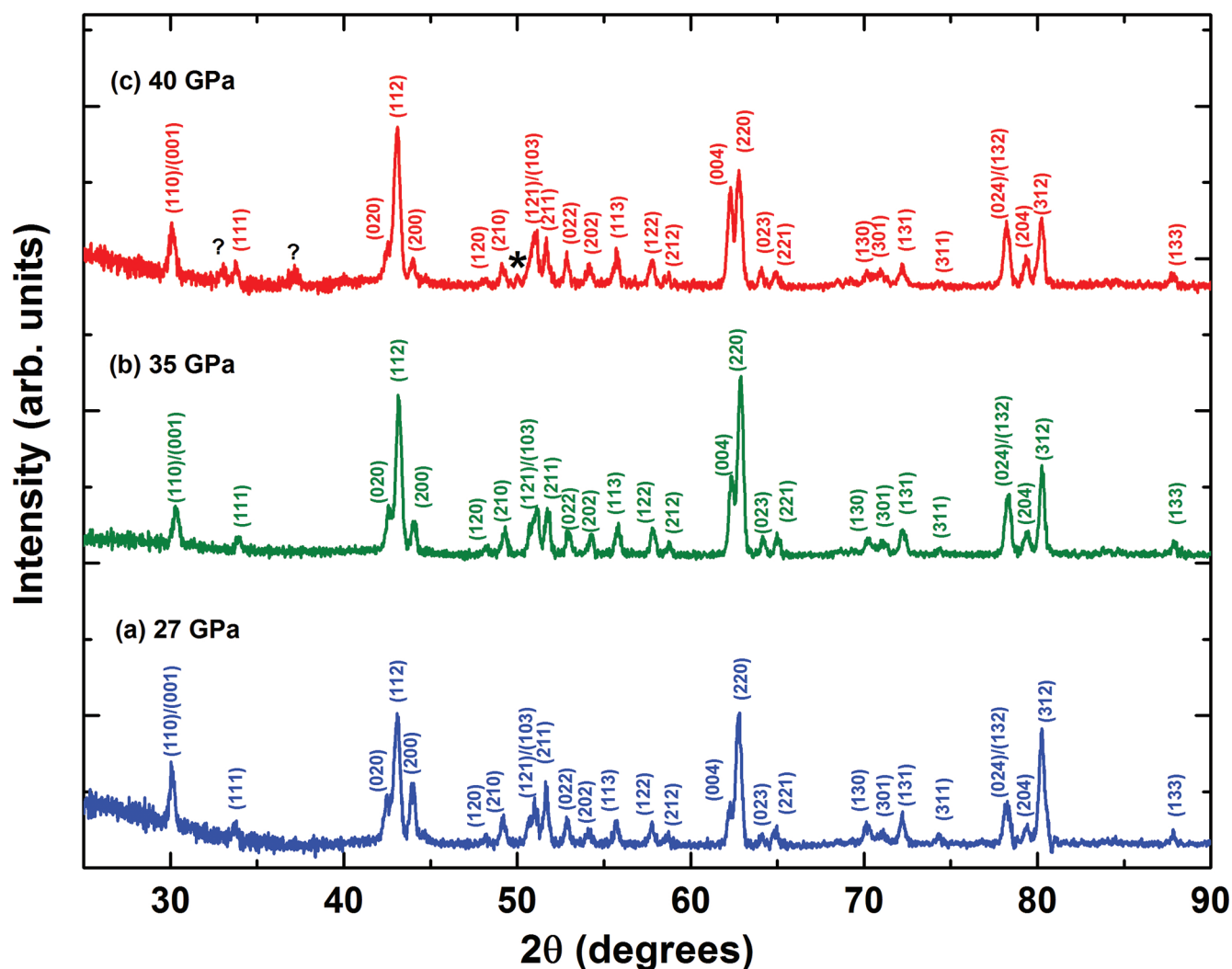


Figure 1 XRD patterns of $\text{En}_{90}\text{Brm}_{10}$ subjected to (a) 27, (b) 35 and (c) 40 GPa and at 2000 °K. Number in parentheses represents the index of bridgmanite. Question marks denote unidentified peaks. Asterisk denotes the probable (200) peak of periclase.

Here, we investigate the solubility of the $\text{MgAlO}_{2.5}$ component in bridgmanite as a function of pressure from 27 to 40 GPa at a constant temperature of 2000 °K and discuss water and noble gas storage capacities in the lower mantle.

Experimental Methods

The starting materials were glasses with $\text{En}_{90}\text{Brm}_{10}$ (En: MgSiO_3 ; Brm: $\text{MgAlO}_{2.5}$; mol. %) and $\text{En}_{95}\text{Cor}_5$ (Cor: Al_2O_3) compositions (see section S-1 in the Supplementary Information for synthesis details and Table S-1 for their compositions). High pressure and high temperature experiments were conducted using ultra-high pressure multi-anvil technology with carbide anvils (Ishii *et al.*, 2016), and detailed techniques can be found in Figures S-1 and S-2 in the Supplementary Information. As shown in Table 1, bridgmanite samples with $\text{En}_{90}\text{Brm}_{10}$ and $\text{En}_{95}\text{Cor}_5$ compositions were first synthesised at 27 GPa and 2000 °K for 3 hours. These samples were annealed at pressures of 35 and 40 GPa and a temperature of 2000 °K for 2 and 3 hours. The recovered samples were analysed by X-ray diffraction (XRD), scanning electron microscopy (SEM), and electron probe microanalysis (EPMA) (see section S-2 in the Supplementary Information for analytical analyses).

Results

XRD patterns of bridgmanite with the $\text{En}_{90}\text{Brm}_{10}$ starting composition synthesised at 27, 35 and 40 GPa are shown in Figure 1, while those for $\text{En}_{95}\text{Cor}_5$ composition are shown in Figure S-3. All diffraction peaks of the sample for the $\text{En}_{90}\text{Brm}_{10}$ composition synthesised at 27 GPa were assigned to those of bridgmanite (Ito and Matsui, 1978), indicating the formation of a single phase bridgmanite. The diffraction peaks of the $\text{En}_{90}\text{Brm}_{10}$ bridgmanite sample annealed at 35 GPa were also assigned to bridgmanite. For the sample annealed at 40 GPa, the majority of its peaks were assigned to bridgmanite, except for three extra weak peaks with d -spacings of 2.11 ($2\theta = 50.3^\circ$), 2.80 ($2\theta = 37.5^\circ$) and 3.15 ($2\theta = 32.9^\circ$) Å. The peak with d -spacing of 3.15 Å was suggested to result from the presence of a superstructure (Navrotsky *et al.*, 2003). The weak peak with d -spacing of 2.11 Å may correspond to (200) of MgO (periclase), which indicates the coexistence of a trace amount of periclase with bridgmanite at 40 GPa and 2000 °K as consistent with the observation by Walter *et al.* (2006). The sample decomposed to periclase and aluminous bridgmanite, suggesting a lower solubility of the $\text{MgAlO}_{2.5}$ component with increasing pressure.

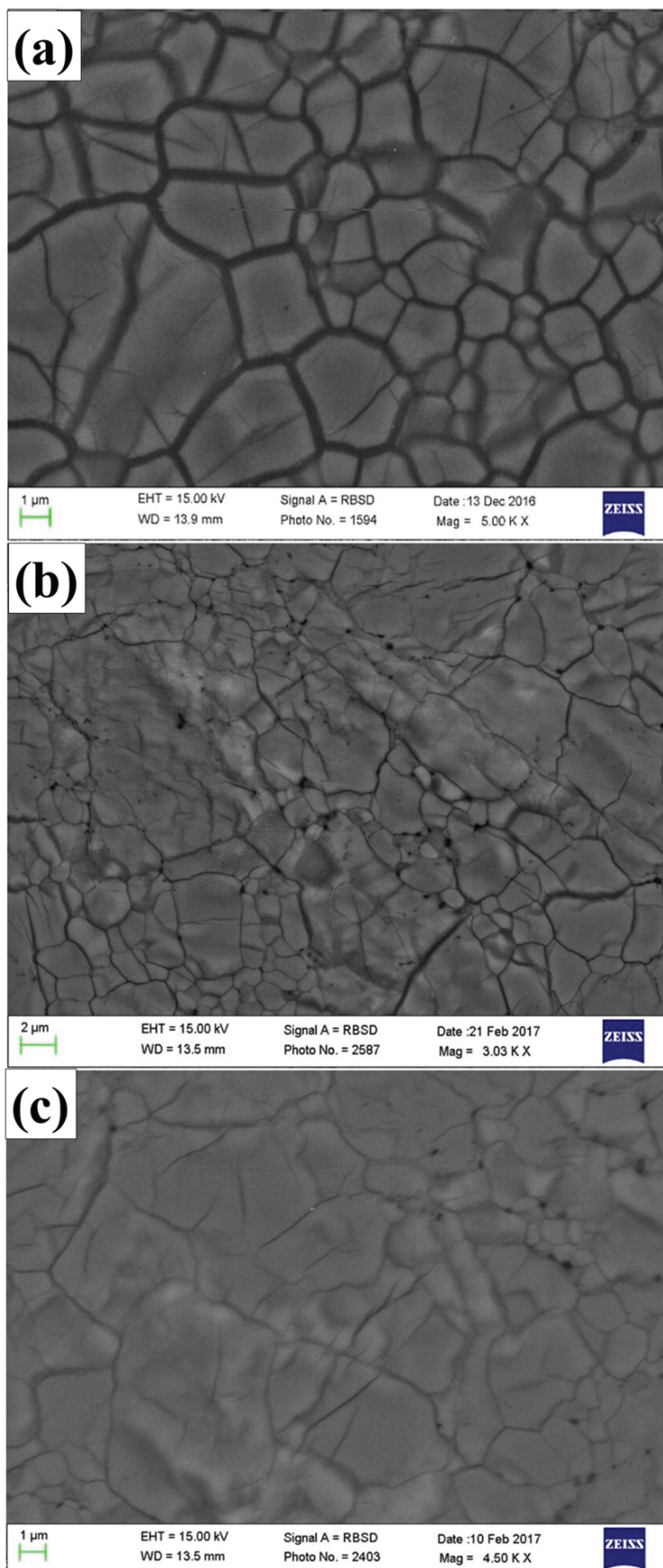


Figure 2 Representative BSE images of $\text{En}_{90}\text{Brm}_{10}$ subjected to (a) 27 GPa, (b) 35 and (c) 40 GPa and 2000 °K.

Textural observations by SEM showed that all samples consist of a single phase. Although the XRD patterns showed the presence of periclase for the sample annealed at 40 GPa, this phase was not detected by back scattered electron (BSE)

observations in Figure 2. Compositions of bridgmanite with grains larger than 3 μm were analysed by EPMA and shown in Table 1, where the total cation numbers were normalised to two to show clearly the variation of oxygen number with pressure.

Table 1 Experimental conditions, run products, and phase compositions.

Start Comp	Phases	MgO	Al ₂ O ₃	SiO ₂	Total	O	Mg	Al	Si
IRIS333 (27 GPa, 2000 °K; 3 hours)									
En ₉₀ Brm ₁₀	Brg [n = 40]	39.82 (23)	5.13 (15)	55.92 (24)	100.86 (14)	2.973 (4)	0.979 (5)	0.100 (3)	0.922 (4)
En ₉₅ Cor ₅	Brg [n = 26]	37.93 (22)	5.11 (12)	56.31 (3)	99.35 (55)	2.998 (2)	0.952 (5)	0.101 (2)	0.948 (4)
IRIS357 (35 GPa, 2000 °K; 2 hours)									
En ₉₀ Brm ₁₀	Brg [n = 52]	39.11 (52)	5.19(13)	56.38 (45)	100.69 (25)	2.984 (7)	0.970 (13)	0.102 (2)	0.938 (7)
IRIS351 (40 GPa, 2000 °K*; 3 hours)									
En ₉₀ Brm ₁₀	Brg [n = 55]	38.01 (40)	5.09 (12)	56.01 (46)	99.11 (65)	2.995 (4)	0.955 (8)	0.101 (2)	0.944 (4)
En ₉₅ Cor ₅	Brg [n = 20]	38.44 (32)	5.12 (16)	57.37 (55)	100.92 (72)	2.999 (3)	0.949 (6)	0.100 (3)	0.950 (3)

Oxide analyses are reported in wt %. n: number of analysis points.

*: temperature was evaluated from a calibrated power curve derived from a lower temperature of 1500 °K.

Number in parentheses represents standard deviation for the last digit (s). Abbreviation: Brg, bridgmanite.

The number of oxygen atoms in bridgmanite from the En₉₀Brm₁₀ and En₉₅Cor₅ compositions in the present and previous studies (Navrotsky *et al.*, 2003; Kojitani *et al.*, 2007) are plotted in Figure 3a. At 27 GPa, the number of oxygens in bridgmanite for the En₉₀Brm₁₀ composition is 2.973 ± 0.004 , which is slightly lower than those in Navrotsky *et al.* (2003) and Kojitani *et al.* (2007) and substantially lower than that of En₉₅Cor₅ bridgmanite. This value shows clearly the presence of oxygen vacancies as consistent with ²⁷Al NMR observations by Stebbins *et al.* (2003). However, the number of oxygens in bridgmanite for the En₉₀Brm₁₀ composition monotonically increases to 2.984 ± 0.007 at 35 GPa, and finally reaches 2.995 ± 0.004 at 40 GPa, which is within the uncertainties of En₉₅Cor₅ bridgmanite at the same pressure, indicating almost no oxygen vacancies at 40 GPa.

Figure 3b shows the variation in the Mg/Si cation ratio in these two kinds of aluminous bridgmanite against pressures. At 27 GPa, this ratio of the sample from the En₉₀Brm₁₀ composition was 1.06 ± 0.01 , which lies between the ideal compositional lines associated with the oxygen-vacancy and charge-coupled substitution. With increasing pressure, it decreases to 1.03 ± 0.02 at 35 GPa, and then to 1.01 ± 0.02 at 40 GPa, which finally lies on the ideal composition line of the charge-coupled substitution for the case of En₉₅Cor₅ bridgmanite.

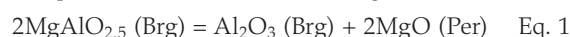
Figure 3c shows the ratios of Al at the A and B sites (Al_B/Al_A) in bridgmanite. This ratio of the sample for En₉₀Brm₁₀ decreases from 3.82 ± 0.53 at 27 GPa to 1.23 ± 0.38 at 40 GPa, which is finally within the uncertainties of unity, the expected result of the charge-coupled substitution. In contrast, this ratio for En₉₅Cor₅ bridgmanite remains almost unchanged with increasing pressure and lies on the line associated with the charge-coupled substitution.

The mass balance calculation implies that 1.2 ± 0.2 and 1.9 ± 0.4 wt. % periclase should coexist with bridgmanite for the En₉₀Brm₁₀ composition at 35 and 40 GPa, respectively. However, XRD patterns exhibited only one peak of periclase from the sample at 40 GPa, and that of the sample at 35 GPa and SEM showed no evidence for the coexistence of periclase. No observation of periclase by SEM could be explained by polishing out tiny interstitial grains.

The results of these observations can be summarised such that the proportion of the MgAlO_{2.5} component in bridgmanite decreases with increasing pressure: 5.7 ± 0.8 mol. % at 27 GPa, 3.2 ± 1.8 mol. % at 35 GPa, and 1.1 ± 1.0 mol. % at 40 GPa (see the detailed calculation in section S-6 in the Supplementary Information). Thus, this component should become negligible at pressures above 40 GPa. Theoretically, the proportion of the MgAlO_{2.5} component should decrease

more rapidly than demonstrated in this study because our starting sample was not ideally saturated with this component (see section S-6 in the Supplementary Information). It is noted that the oxygen fugacity has a negligible effect on the oxygen vacancy for Fe-free minerals (*e.g.*, Smyth and Stocker, 1975; Stocker and Smyth, 1978). Compositions of synthetic Al-bearing bridgmanite being consistent with each other by using different metal capsules (such as gold and rhenium) and also comparable to those of the glass starting materials in the present and previous studies (Navrotsky *et al.*, 2003; Kojitani *et al.*, 2007) further confirms this point. Therefore, pressure is the only factor to result in this rapid decrease of the MgAlO_{2.5} component in bridgmanite.

The present conclusion can be understood by a simple volume comparison based on the following reaction:



The molar volume of periclase (Per) under ambient conditions is 11.27 cm³/mole. The molar volumes of the hypothetical end members of MgAlO_{2.5} and Al₂O₃ bridgmanite (for Al cation number of 0.1 *per* formula unit) under ambient conditions are estimated to be 24.50 and 24.54 cm³/mole, respectively, from the volume composition data in Figure S-4 and Liu *et al.* (2016). Therefore, the molar volume of the left hand side component of Equation 1 is larger than that of the right hand side components by 1.92 cm³/mole, suggesting that the MgAlO_{2.5} component becomes unstable with increasing pressure (see Fig. S-5).

Geochemical Implications

Although the water storage of the lower mantle is uncertain, it has significant impacts on the chemical evolution of the mantle. The oxygen vacancy substitution, one of the most likely mechanisms, in aluminous bridgmanite may provide suitable storage sites to incorporate water in the shallower part of the lower mantle (*e.g.*, Navrotsky, 1999; Brodholt, 2000) according to the following reaction:



Although the volume of the MgHAIO₃ component in bridgmanite is unknown, we could assume that it has a similar volume with the MgAlO_{2.5} component because of an actually zero volume of the proton (Hernández *et al.*, 2013). Hence, H₂O is expected to be incorporated in bridgmanite as MgHAIO₃ in the lower mantle because of high pressures. Murakami *et al.* (2002) and Litasov *et al.* (2003) reported that synthetic Al-Fe-bearing bridgmanite in mantle peridotite can contain 1000–2000 ppm water at 26 GPa and 1500–1923 °K, which is significantly higher than that in synthetic MgSiO₃ bridgmanite at 24–25 GPa and 1573–1873 °K (Bolfan-Casanova *et al.*, 2000;



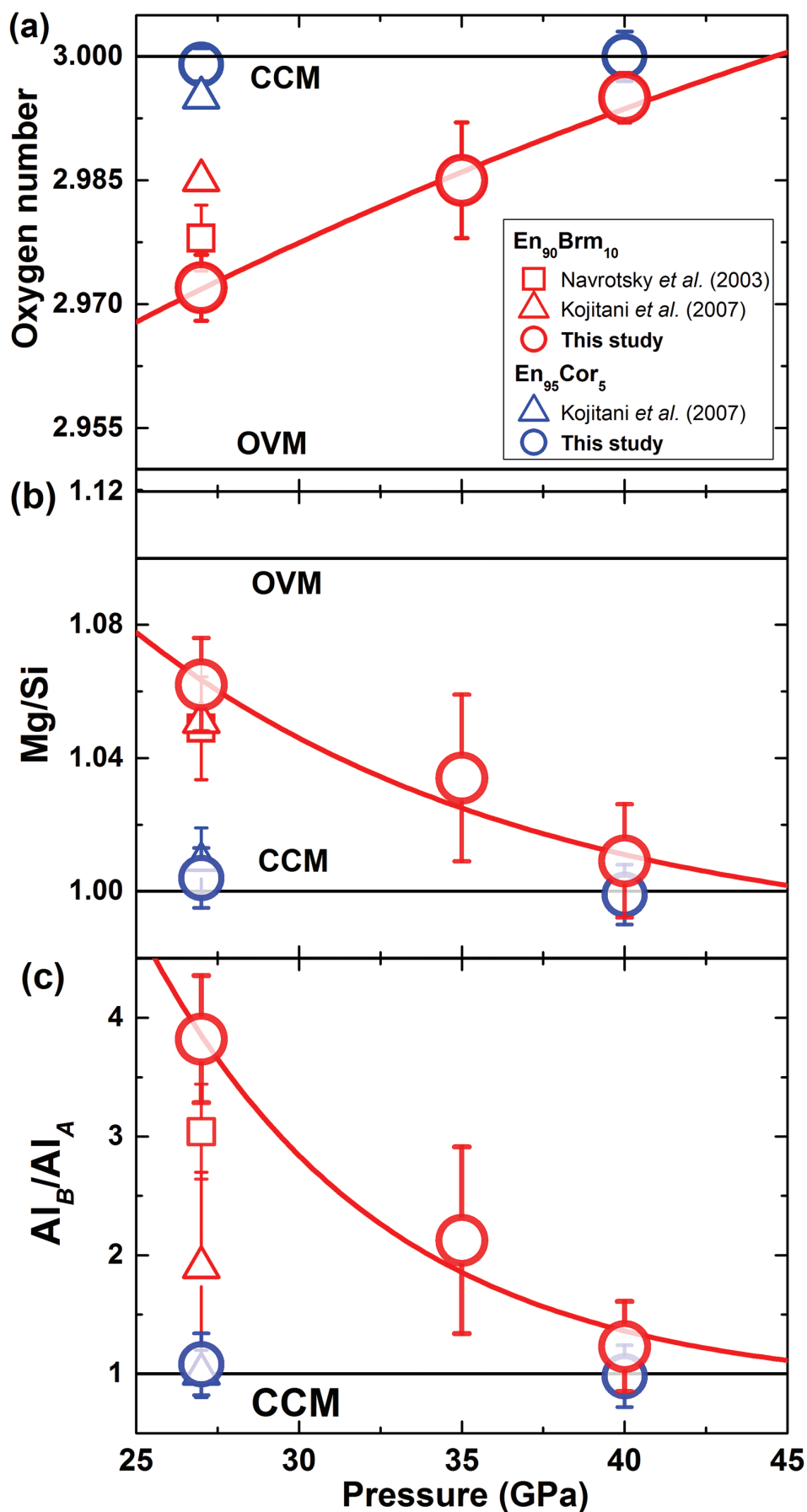


Figure 3 Plots of (a) oxygen number, (b) Mg/Si ratio, and (c) Al ratio in A and B sites (Al_B/Al_A) in bridgmanite for $En_{90}Brm_{10}$ and $En_{95}Cor_5$ versus pressure. The black lines represent the compositions associated with the oxygen-vacancy substitution mechanism (OVM) and charge-coupled substitution mechanism (CCM) for bridgmanite. The red line is the least squares fitting ($Mg/Si = A_{exp}(-P/B) + C$, where P is pressure) of the present data.

Litasov *et al.*, 2003). Following Equation 2, the amount of 2.2 mol. % MgAlO_{2.5} in bridgmanite can explain those reported high water amounts in bridgmanite. In contrast, Bolfan-Casanova *et al.* (2003) and Panero *et al.* (2015) showed that Al-Fe-bearing bridgmanite had a very low water content (<10 ppm) at 24–26 GPa and 1600–2000 °K. Even though bridgmanite contained these amounts of water in their experimental conditions, the water solubility should rapidly decrease with increasing pressure due to a rapid decrease of MgAlO_{2.5} component in bridgmanite. Since bridgmanite has a negligible MgAlO_{2.5} component at pressures above 40 GPa, no water could be stored in regions deeper than 1000 km depth, *i.e.* in the majority of the lower mantle. Furthermore, the ambient lower mantle temperatures (Katsura *et al.*, 2010) are too high for hydrous minerals (Walter *et al.*, 2015), therefore, we conclude that the majority of lower mantle is dry.

Shcheka and Keppler (2012) showed that MgSiO₃ bridgmanite contained ~1 wt. % argon at 25 GPa and 1873–2073 °K dissolved through oxygen-vacancy substitution. Theoretically, Al-bearing bridgmanite may accommodate larger amounts of argon than MgSiO₃ bridgmanite because of the higher proportion of oxygen vacancies in the uppermost part of the lower mantle. With increasing depths, the incorporation capacity of argon quickly diminishes, due to the rapidly decreasing oxygen vacancies in aluminous bridgmanite, and finally vanishes at depths deeper than 1000 km. Therefore, the explanation for the xenon anomaly in the Earth's atmosphere given by Shcheka and Keppler (2012) needs to be further investigated.

Bridgmanite, the most abundant phase in the lower mantle (80 vol. %; Irifune, 1994), dominates the viscosity of this region (Girard *et al.*, 2016). Seismic observation suggests that some slabs stagnate at 600–1000 km depths (Fukao and Obayashi, 2013). Since there are no phase transitions in this region, some special explanations are required. One explanation is the increase of viscosity with depth in this region. Since the viscosity of minerals is controlled by atomic diffusivity (Karato and Wu, 1993), the decrease of oxygen-vacancies in aluminous bridgmanite will cause a decrease in element diffusivity. Therefore, the expected decrease in diffusivity for aluminous bridgmanite should cause a high viscosity, which may explain this mid-lower mantle slab stagnation.

Acknowledgements

The authors thank D. Krauß for his technical assistance in electron microprobe analysis. We also thank H. Fei, S. Shcheka and L. Wang for their fruitful discussion and comments. The authors thank S. Redfern for editing this manuscript, and two anonymous reviewers for their constructive comments. Z. L. was financially supported by the Bayerisches Geoinstitut Visitor's Program. This study is also supported by research grants to T. K. (BMBF: 05K13WC2, 05K13WC2; DFG: KA3434/3-1, KA3434/7-1, KA3434/8-1, KA3434/9-1).

Editor: Simon Redfern

Additional Information

Supplementary Information accompanies this letter at www.geochemicalperspectivesletters.org/article1739

Reprints and permission information are available online at <http://www.geochemicalperspectivesletters.org/copyright-and-permissions>

Cite this letter as: Liu, Z., Ishii, T., Katsura, T. (2017) Rapid decrease of MgAlO_{2.5} component in bridgmanite with pressure. *Geochem. Persp. Let.* 5, 12–18.

References

- AKBER-KNUTSON, S., BUKOWINSKI, M.S.T. (2004) The energetics of aluminum solubility into MgSiO₃ perovskite at lower mantle conditions. *Earth and Planetary Science Letters* 220, 317–330.
- BOLFAN-CASANOVA, N., KEPPLER, H., RUBIE, D.C. (2000) Water partitioning between nominally anhydrous minerals in MgO-SiO₂-H₂O system up to 24 GPa: implications for the distribution of water in the Earth's mantle. *Earth and Planetary Science Letters* 182, 209–221.
- BOLFAN-CASANOVA, N., KEPPLER, H., RUBIE, D.C. (2003) Water partitioning at 660 km depth and evidence for very low water solubility in magnesium silicate perovskite. *Geophysical Research Letters* 30, 1905.
- BRODHOLT, J.P. (2000) Pressure-induced changes in the compression mechanism of aluminous perovskite in the Earth's mantle. *Nature* 407, 620–622.
- FUKAO, Y., OBAYASHI, M. (2013) Subducted slabs stagnate above, penetrating through, and trapped below the 660 km discontinuity. *Journal of Geophysical Research: Solid Earth* 118, 2013JB010466.
- GIRARD, J., AMULELE, G., FARLA, R., MOHIUDDIN, A., KARATO, S.-I. (2016) Shear deformation of bridgmanite and magnesio-wüstite aggregates at lower mantle conditions. *Science* 351, 144–147.
- HERNÁNDEZ, E., ALFÈ, D., BRODHOLT, J. (2013) The incorporation of water into lower-mantle perovskites: a first-principles study. *Earth and Planetary Science Letters* 364, 37–43.
- HIRSCH, L.M., SHANKLAND, T.J. (1991) Point defects in silicate perovskite. *Geophysical Research Letters* 18, 1305–1308.
- IRIFUNE, T. (1994) Absence of an aluminous phase in the upper part of the Earth's lower mantle. *Nature* 370, 131–133.
- ISHII, T., SHI, L., HUANG, R., TSUJINO, N., DRUZHBIN, D., MYHILL, R., LI, Y., WANG, L., YAMAMOTO, T., MIYAJIMA, N., KAWAZOE, T., NISHIYAMA, N., HIGO, Y., TANGE, Y., KATSURA, T. (2016) Generation of pressure over 40 GPa using Kawai-type multi-anvil press with tungsten carbide anvils. *Review of Scientific Instruments* 87, 024501-1–024501-6.
- ITO, E., MATSUI, Y. (1978) Synthesis and crystal-chemical characterization of MgSiO₃ perovskite. *Earth and Planetary Science Letters* 38, 443–450.
- KARATO, S., WU, P. (1993) Rheology of the upper mantle: a synthesis. *Science* 260, 771–778.
- KATSURA, T., YONEDA, A., YAMAZAKI, D., YOSHINO, T., ITO, E. (2010) Adiabatic temperature profile in the mantle. *Physics of the Earth and Planetary Interiors* 183, 212–218.
- KOJITANI, H., KATSURA, T., AKAOGI, M. (2007) Aluminum substitution mechanisms in perovskite-type MgSiO₃: an investigation by Rietveld analysis. *Physics and Chemistry of Minerals* 34, 257–267.
- LITASOV, K., OHTANI, E., LANGENHORST, F., YURIMOTO, H., KUBO, T., KONDO, T. (2003) Water solubility in Mg-perovskites and water storage capacity in the lower mantle. *Earth and Planetary Science Letters* 211, 189–203.
- LIU, Z.D., IRIFUNE, T., NISHI, M., TANGE, Y., ARIMOTO, T., SHINMEI, T. (2016) Phase relations in the system MgSiO₃-Al₂O₃ up to 52 GPa and 2000 K. *Physics of the Earth and Planetary Interiors* 257, 18–27.
- MCDONOUGH, W.F., SUN, S.-S. (1995) The composition of the Earth. *Chemical Geology* 120, 223–253.
- MURAKAMI, M., HIROSE, K., YURIMOTO, H., NAKASHIMA, S., TAKAFUJI, N. (2002) Water in Earth's lower mantle. *Science* 295, 1885–1887.
- NAVROTSKY, A. (1999) A lesson from ceramics. *Science* 284, 1788–1789.
- NAVROTSKY, A., SCHOENITZ, M., KOJITANI, H., XU, H., ZHANG, J., WEIDNER, D.J., JEANLOZ, R. (2003) Aluminum in magnesium silicate perovskite: Formation, structure, and energetics of magnesium-rich defect solid solutions. *Journal of Geophysical Research* 108, 2330.
- PANERO, W.R., PIGOTT, J.S., REAMAN, D.M., KABBES, J.E., LIU, Z. (2015) Dry (Mg,Fe)SiO₃ perovskite in the Earth's lower mantle. *Journal of Geophysical Research* 120, 894–908.
- SHCHEKA, S.S., KEPPLER, H. (2012) The origin of the terrestrial noble-gas signature. *Nature* 490, 531–534.
- SMYTH, D.M., STOCKER, R.L. (1975) Point defects and non-stoichiometry in forsterite. *Physics of the Earth and Planetary Interiors* 10, 183–193.
- STEBBINS, J.F., KOJITANI, H., AKAOGI, M., NAVROTSKY, A. (2003) Aluminum substitution in MgSiO₃ perovskite: Investigation of multiple mechanisms by ²⁷Al NMR. *American Mineralogist* 88, 1161–1164.



- STOCKER, R.L., SMYTH, D.M. (1978) Effect of enstatite activity and oxygen partial pressure on the point-defect chemistry of olivine. *Physics of the Earth and Planetary Interiors* 16, 146–156.
- WALTER, M., TRONNES, R.G., ARMSTRONG, L.S., LORD, O., CALDWELL, W.A., CLARK, A.M. (2006) Subsolidus phase relations and perovskite compressibility in the system MgO–AlO_{1.5}–SiO₂ with implications for Earth's lower mantle. *Earth and Planetary Science Letters* 248, 77–89.
- WALTER, M.J., THOMSON, A.R., WANG, W., LORD, O.T., ROSS, J., MCMAHON, S.C., BARON, M.A., MELEKHOVA, E., KLEPPE, A.K., KOHN, S.C. (2015) The stability of hydrous silicates in Earth's lower mantle: Experimental constraints from the systems MgO–SiO₂–H₂O and MgO–Al₂O₃–SiO₂–H₂O. *Chemical Geology* 418, 16–29.
- YAMAMOTO, T., YUEN, D.A., EBISUZAKI, T. (2003) Substitution mechanism of Al ions in MgSiO₃ perovskite under high pressure conditions from first-principles calculations. *Earth and Planetary Science Letters* 206, 617–625.
- ZHANG, J., WEIDNER, D.J. (1999) Thermal equation of state of aluminum-enriched silicate perovskite. *Science* 284, 782–784.



Rapid decrease of MgAlO_{2.5} component in bridgmanite with pressure

Z. Liu^{1*}, T. Ishii¹, T. Katsura¹

Supplementary Information

The Supplementary Information includes:

- 1. Glass Preparation
- 2. High Pressure Technique in Kawai-type Multi-anvil Apparatus
- 3. Analytical Methods
- 4. XRD of En₉₅Cor₅-bridgmanite at 27 and 40 GPa and 2000 °K
- 5. Unit Cell Volume of Bridgmanite
- 6. Calculation of the Solubility of the MgAlO_{2.5} Component in Bridgmanite
- 7. The Variation of Molar Volume for Equation S-1
- Figures S-1 to S-5
- Tables S-1 to S-3
- Supplementary Information References

1. Glass Preparation

Besides with En₉₀Brm₁₀ and En₉₅Cor₅ glass, En₁₀₀ glass is also prepared for the standard for composition comparison. All glasses were prepared from oxide mixtures using reagent grade chemicals: MgO, SiO₂, and Al₂O₃, fused and homogenised at least two times at 2000 °K for one hour, and finally quenched into water. After that, the glasses were finely ground into powder, then checked by powder X-ray diffraction to confirm absence of solid phases. They were finally kept in a high vacuum box before experiments. Based on the compositions in Table S-1, the total cation number is normalised to two to see oxygen vacancies clearly in the

starting material. Therefore, the composition of the En₉₀Brm₁₀ glass is Mg_{0.982±0.006}Al_{0.101±0.001}Si_{0.918±0.003}O_{2.969±0.003}, which clearly deviates from the Al₂O₃ stoichiometry and is deficient in oxygen. This glass starting material contains about 6.4 ± 0.9 mol. % MgAlO_{2.5} and 1.9 ± 0.5 mol. % AlO_{1.5}, which is slightly smaller than that with the nominal MgAlO_{2.5} component of En₉₀Brm₁₀. Therefore the starting material is not ideally saturated with MgAlO_{2.5} as En₉₀Brm₁₀. Here, we approximated this non-stoichiometric glass starting material with Mg_{0.982±0.006}Al_{0.101±0.001}Si_{0.918±0.003}O_{2.969±0.003} as En₉₀Brm₁₀-glass. The En₁₀₀ and En₉₅Cor₅ glasses have the intended compositions within analytical errors.

Table S-1 Chemical compositions of the starting glass material.

Starting material	MgO	Al ₂ O ₃	SiO ₂	Total	O	Mg	Al	Si
En ₉₀ Brm ₁₀ (n = 25)	39.49 (18)	5.11 (5)	55.08 (37)	99.68 (40)	2.969 (3)	0.982 (6)	0.101 (1)	0.918 (3)
En ₉₅ Cor ₅ (n = 15)	38.42 (29)	5.10 (5)	57.47 (48)	100.99 (52)	3.002 (7)	0.948 (9)	0.100 (2)	0.951 (7)
En ₁₀₀ (n = 12)	40.03 (50)	–	59.48 (60)	99.39 (36)	2.998 (3)	1.001 (9)	–	0.999 (7)

Oxide analyses are reported in wt. %. n: number of analysis points.
Number in parentheses represents standard deviation and is placed in the last digit (s).

1. Bayerisches Geoinstitut, University of Bayreuth, 95440 Bayreuth, Germany
* Corresponding author (email: zhaodong.liu@uni-bayreuth.de)



2. High Pressure Technique in Kawai-type Multi-anvil Apparatus

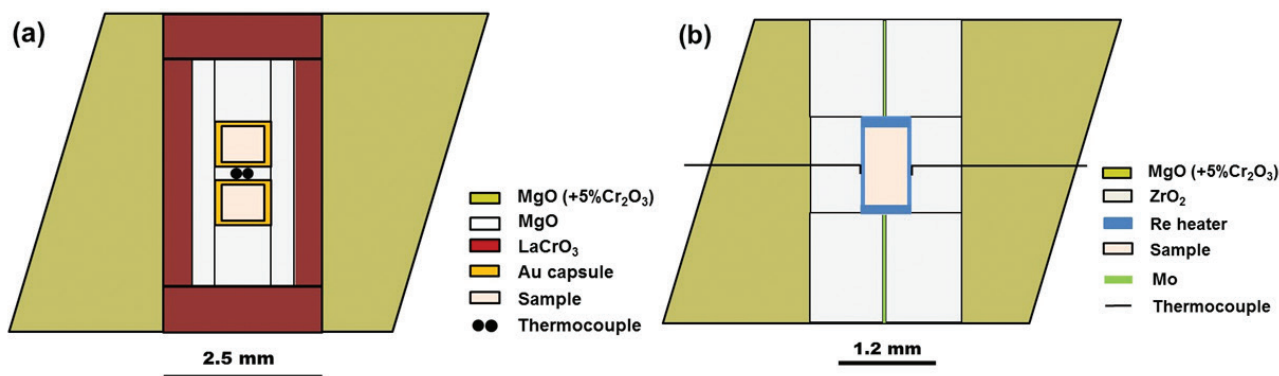


Figure S-1 The schematic illustration of (a) 7/3 and (b) 5.7/1.5 cell assembly for high pressure and high temperature experiments.

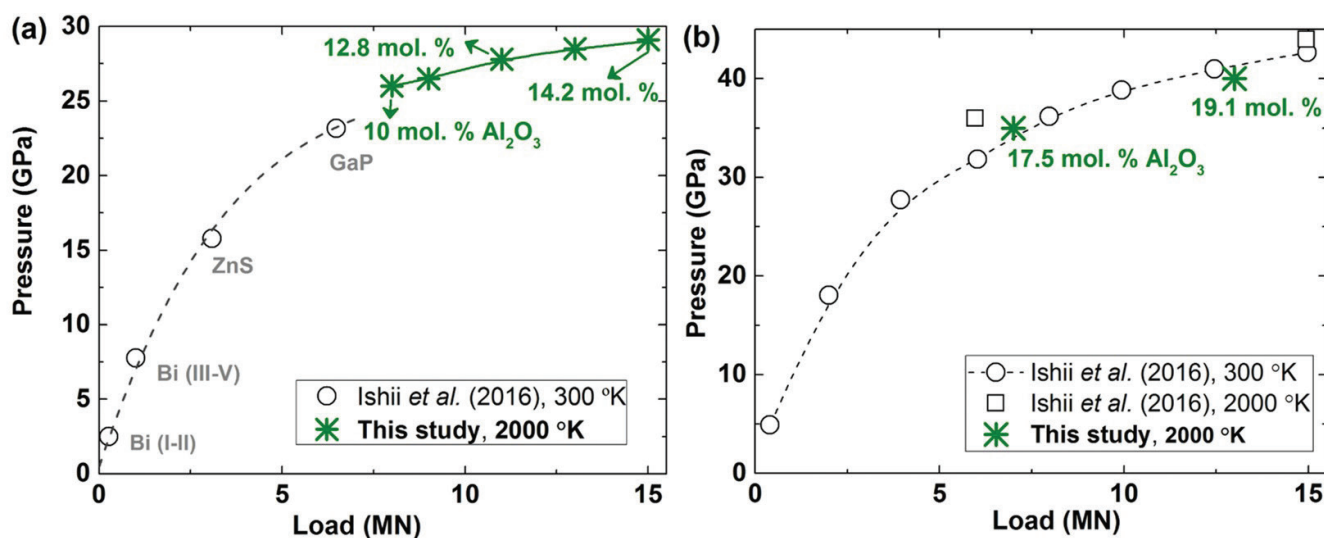


Figure S-2 Pressure calibrations of 7/3 (a) and 5.7/1.5 (b) cell assembly in IRIS-15 at 300 and 2000 °K, respectively.

Bridgmanite samples were first synthesised at a pressure of 27 GPa and a temperature of 2000 °K for 3 hours using a 7/3 (OEL/TEL = octahedral edge length of pressure medium/truncated edge length of anvil) cell assembly (Fig. S-1a) in a Kawai-type multi-anvil apparatus (IRIS-15) with a DIA-type guide block and a maximum press load of 15 MN in Bayerisches Geoinstitut, University of Bayreuth, Germany. After that, the bridgmanite samples were cut into two parts for X-ray diffraction, scanning electron microscopy and electron probe microanalysis, respectively.

Furthermore, two annealing high pressure experiments are conducted at pressures of 35 and 40 GPa, respectively, and a temperature of 2000 °K for 2 and 3 hours using a synthetic single phase non-stoichiometric bridgmanite (hereafter as $\text{En}_{90}\text{Brm}_{10}\text{-Brg}$), which was synthesised from the starting $\text{En}_{90}\text{Brm}_{10}$ glass at 27 GPa and 2000 °K, as a starting material in a 5.7/1.5 cell assembly (Fig. S-1b) by means of the ultra-high pressure multi-anvil technology (Ishii *et al.*, 2016). The 7/3 and 5.7/1.5 cell assemblies are shown in Figure S-1, and LaCrO_3 and rhenium (Re) were used for the heaters in these two cell assemblies, respectively. Pressure calibrations of these two cell assemblies at room temperature and high temperature were reported by Ishii *et al.* (2016), and also shown in Figure S-2 based on the Al_2O_3 solubility in bridgmanite (Liu *et al.*, 2016). The pressure uncertainty of 7/3 cell assembly is ± 0.5 GPa (Ishii *et al.*, 2016), while that for 5.7/1.5 is ± 1 GPa based on the

uncertainties of Al_2O_3 solubility in bridgmanite. Temperature was measured with a $\text{W}_{97}\text{Re}_3\text{-W}_{75}\text{Re}_{25}$ thermocouple adjacent to the sample capsules. In experiments where no direct temperature reading from the thermocouple was obtained, temperatures were estimated using power-temperature relationships established by preceding runs.

3. Analytical Methods

Phases in recovered samples were identified using a micro-focused X-ray diffractometer with a Co anode operated at 40 kV, 500 μA . MgSiO_3 bridgmanite, synthesised in the IRIS333 run (Table S-2), was used as the external standard to calibrate the Bragg angle (2θ) of the instrument. XRD profiles were collected for about one hour. Electron back scattered images were collected by a LEO1530 scanning electron microscope operating at an acceleration voltage of 15 kV and a beam current of 10 nA. Chemical compositions were determined by a JEOL JXA-8200 electron probe microanalyser (EPMA) operating at 15 kV and 5 nA with standards of enstatite for Mg and Si, and pyrope for Al.

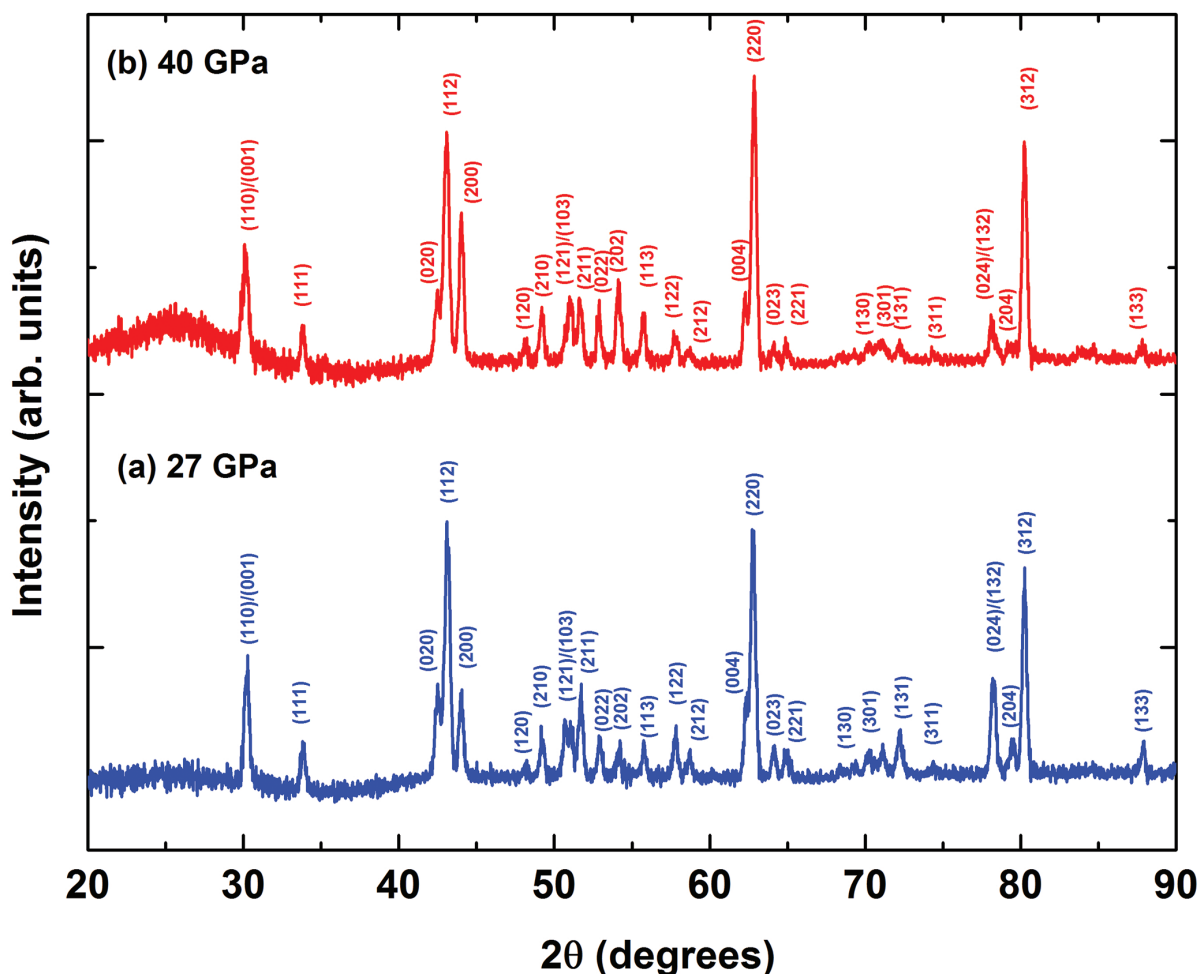


Figure S-3 XRD patterns of the recovered sample for $\text{En}_{95}\text{Cor}_5$ composition at 27 (a) and 40 GPa (b) under 2000 °K, respectively. Number in parentheses represents the index of bridgmanite.

Table S-2 The experimental condition and composition of MgSiO_3 bridgmanite.

Starting material	Phases	MgO	Al_2O_3	SiO_2	Total	O	Mg	Al	Si
IRIS333 (27 GPa, 2000 °K; 3 hours)									
En_{100}	Brg (n = 25)	40.16 (37)	–	59.72 (37)	99.88 (35)	2.999 (7)	1.000 (3)	–	1.001 (7)

Oxide analyses are reported in wt. %. n: number of analysis points.

Number in parentheses represents standard deviation and is placed in the last digit (s).

Abbreviation: Brg, bridgmanite.

4. XRD of $\text{En}_{95}\text{Cor}_5$ -bridgmanite at 27 and 40 GPa and 2000 °K

Figure S-3a shows XRD patterns for synthetic $\text{En}_{95}\text{Cor}_5$ -bridgmanite at pressures of 27 GPa and 2000 °K, and Figure S-3b shows that for the annealing sample for $\text{En}_{95}\text{Cor}_5$ -bridgmanite at 40 GPa and 2000 °K. Their compositions are almost consistent with that of starting glass, indicating that bridgmanite is the only phase in these recovered samples.

5. Unit Cell Volume of Bridgmanite

Figure S-4 shows unit cell volumes of bridgmanite along the system MgSiO_3 - Al_2O_3 and MgSiO_3 - $\text{MgAlO}_{2.5}$ in the present and previous studies (Ito and Matsui, 1978; Weng *et al.*, 1981; Irifune *et al.*, 1996; Kubo and Akaogi, 2000; Navrotsky *et al.*, 2003; Walter *et al.*, 2004, 2006; Kojitani *et al.*, 2007). In the present study, unit cell volumes of the recovered bridgmanite

for the $\text{En}_{90}\text{Brm}_{10}$ composition at 35 and 40 GPa are slightly lower than those at 27 GPa under the same temperature of 2000 °K, but comparable with those of bridgmanite for $\text{En}_{95}\text{Cor}_5$ composition within analytical uncertainties in the present study. This may be caused by the slight change of the crystal chemistry for bridgmanite or the stress in these recovered samples at different pressures. Moreover, these volumes of the recovered bridgmanite for the $\text{En}_{90}\text{Brm}_{10}$ composition in the present study are comparable to those of previous studies on the same composition within analytical uncertainties (Navrotsky *et al.*, 2003; Walter *et al.*, 2006; Kojitani *et al.*, 2007), which is also within uncertainties of bridgmanite for $\text{En}_{95}\text{Cor}_5$ composition in previous studies (Weng *et al.*, 1981; Irifune *et al.*, 1996; Kubo and Akaogi, 2000; Walter *et al.*, 2004). The largely scattered value for bridgmanite with the same composition may be caused by the different synthesis conditions, quench history, and analytical methods.

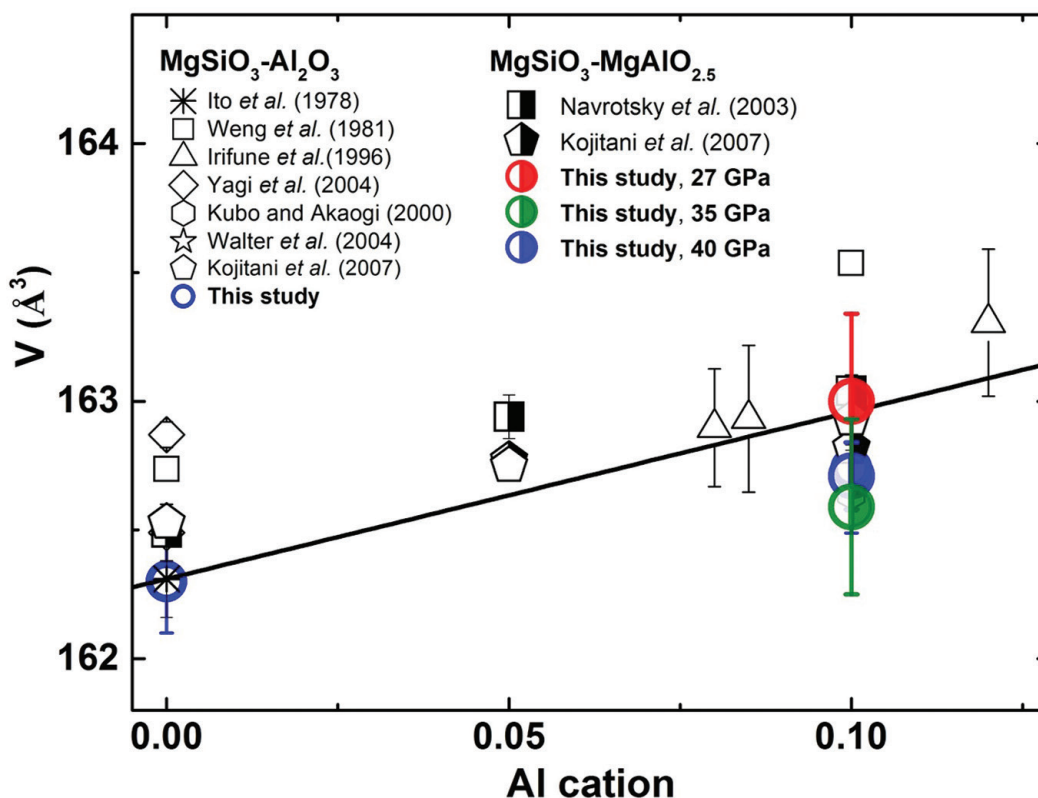
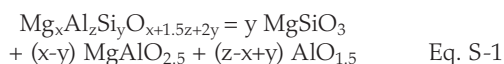


Figure S-4 Unit cell volumes of bridgmanite along the system $\text{MgSiO}_3\text{-Al}_2\text{O}_3$ and $\text{MgSiO}_3\text{-MgAlO}_{2.5}$ in the present and previous studies. The solid line presents the linear fitting results on values for bridgmanite along the system $\text{MgSiO}_3\text{-Al}_2\text{O}_3$ (Liu *et al.*, 2016).

6. Calculation of the Solubility of the $\text{MgAlO}_{2.5}$ Component in Bridgmanite

It is known that both $\text{MgAlO}_{2.5}$ (the oxygen-vacancy substitution) and $\text{AlO}_{1.5}$ (the charge-coupled substitution) are competing with each other in aluminous bridgmanite in both systems $\text{MgSiO}_3\text{-MgAlO}_{2.5}$ and $\text{-AlO}_{1.5}$, therefore, the composition of bridgmanite can be represented by the following reaction:

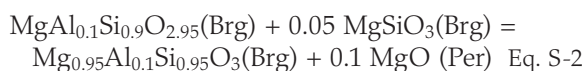


Following this equation, the composition of bridgmanite in Table S-2 can be well calculated using the $\text{MgAlO}_{2.5}$ and $\text{AlO}_{1.5}$, and thus the solubility of $\text{MgAlO}_{2.5}$ in bridgmanite can be derived.

It is noted that the equilibrated proportion at 27 GPa could be higher because our sample at this condition was not ideally saturated with the $\text{MgAlO}_{2.5}$ component for the glass starting material. On the other hand, the equilibrated proportions at 35 and 40 GPa could be lower, because the starting material was bridgmanite that had more $\text{MgAlO}_{2.5}$ component than the present run products. Therefore the proportion of the $\text{MgAlO}_{2.5}$ component should decrease more rapidly than demonstrated in this study.

7. The Variation of Molar Volume for Equation 1

Considering Al cation number of 0.1 for the Equation 1 in the main text based on the present and previous studies, the Eq. 1 can be represented by the following chemical equation:



Pressure and temperature effects on molar volume are calculated using the third order Birch–Murnaghan equation:

$$P = \left(\frac{3K_T}{2} \right) \left[\left(\frac{V_{0T}}{V} \right)^{\frac{7}{3}} - \left(\frac{V_{0T}}{V} \right)^{\frac{5}{3}} \right] \left[1 + \frac{3}{4} (K'_T - 4) \left[\left(\frac{V_{0T}}{V} \right)^{\frac{2}{3}} - 1 \right] \right] \quad \text{Eq. S-3}$$

where K_T , V_{0T} , V , and K'_T are the isothermal bulk modulus, zero pressure molar volume, high pressure molar volume and pressure derivative of bulk modulus. The temperature effects for K_T and V_{0T} are given by:

$$K_T = K_0 + \left(\frac{\partial K_T}{\partial T} \right) (T - T_0) \quad \text{Eq. S-4}$$

$$V_{0T} = V_0 \exp \left[\int_{T_0}^T \alpha_T dT \right] \quad \text{Eq. S-5}$$

where $(\partial K_T / \partial T)_P$, T_0 , V_0 and α are the temperature derivatives of the bulk modulus, reference temperature, molar volume and volumetric thermal expansion at ambient pressure, respectively. Thermal expansion α is empirically represented by

$$\alpha_T = a_0 + a_1 T + a_2 T^2 \quad \text{Eq. S-6}$$

The experimental thermoelastic parameters of these mantle minerals used in Equation S-2 are shown in Table S-3.

The calculated ΔV as a function of pressure is shown in Figure S-5 under 300 and 2000 °K, respectively. It is seen that the values of ΔV are minus at both temperatures at 27–50 GPa, suggesting the pressure would enhance both Equations 1 and S-2 from the left to right direction. Therefore, the pressure will decrease the component of $\text{MgAlO}_{2.5}$ in bridgmanite.



Table S-3 Elastic properties of minerals related with Eq. S-2 used for thermodynamic calculations.

Phase	MgSiO ₃ -Brg	Mg _{0.95} Al _{0.1} Si _{0.95} O ₃ -Brg	MgAl _{0.1} Si _{0.9} O _{2.95} -Brg	MgO
V ₀ (cm ³ /mol)	24.44 (1) ^a	24.54 (1) ^e	24.50 (1) ^f	11.27 (1) ^h
ΔH ₀ (KJ/mol)	10.79 (196) ^b	16.44 (88) ^b	10.24 (428) ^f	36.48 (50) ⁱ
ΔS ₀ (KJ/mol)	0.063 ^b	0.058 ^b	0.073 ^f	0.026 ⁱ
K _{T298} (GPa)	256.7 (15) ^a	239 (1) ^e	259 (8) ^g	160.9 ^h
K' _T	4.09 (6) ^a	4 ^e	4 ^g	4.35 (10) ^h
(∂K _T /∂T) _P (GPa/°K)	-0.035 (2) ^c	-0.057 (1) ^e	-0.057 (1) [*]	-0.0272 ^h
$\alpha_\tau = a_0 + a_1T + a_2T^2$ (oK ⁻¹)				
a ₀ × 10 ⁵	1.982 ^d	2.08 (26) ^e	2.08 (26) [*]	3.38 ⁱ
a ₁ × 10 ⁸	0.818 ^d	2.21 (67) ^e	2.21 (67) [*]	12.52 ⁱ
a ₂ × 10	-4.740 ^d	0	0	-19.13 ⁱ
$C_p = A + BT^{-0.5} + CT^{-2}$ (oK ⁻¹)				
A × 10 ⁻²	1.769 ^d	1.769 [#]	1.769 [*]	0.66 ⁱ
B × 10 ⁻³	-1.565 ^d	-1.565 [#]	-1.565 [*]	-0.36 ⁱ
C × 10 ⁻⁶	0	0	0	-0.61 ⁱ

a: Tange *et al.* (2012)

b: Akaogi and Ito (1999)

c: Katsura *et al.* (2009)

d: Funamori *et al.* (1996)

e: Zhand and Wiedner (1999)

f: Navrotsky *et al.* (2003)

g: Walter *et al.* (2006)

h: Kono *et al.* (2010)

i: Kojitani *et al.* (2012)

#: the same value with that of MgSiO₃-Brg.

*: the same value with that of Mg_{0.95}Al_{0.1}Si_{0.95}O₃-Brg

Abbreviation: Brg: bridgmanite.

Number in parentheses represents standard deviation and is placed in the last digit (s).

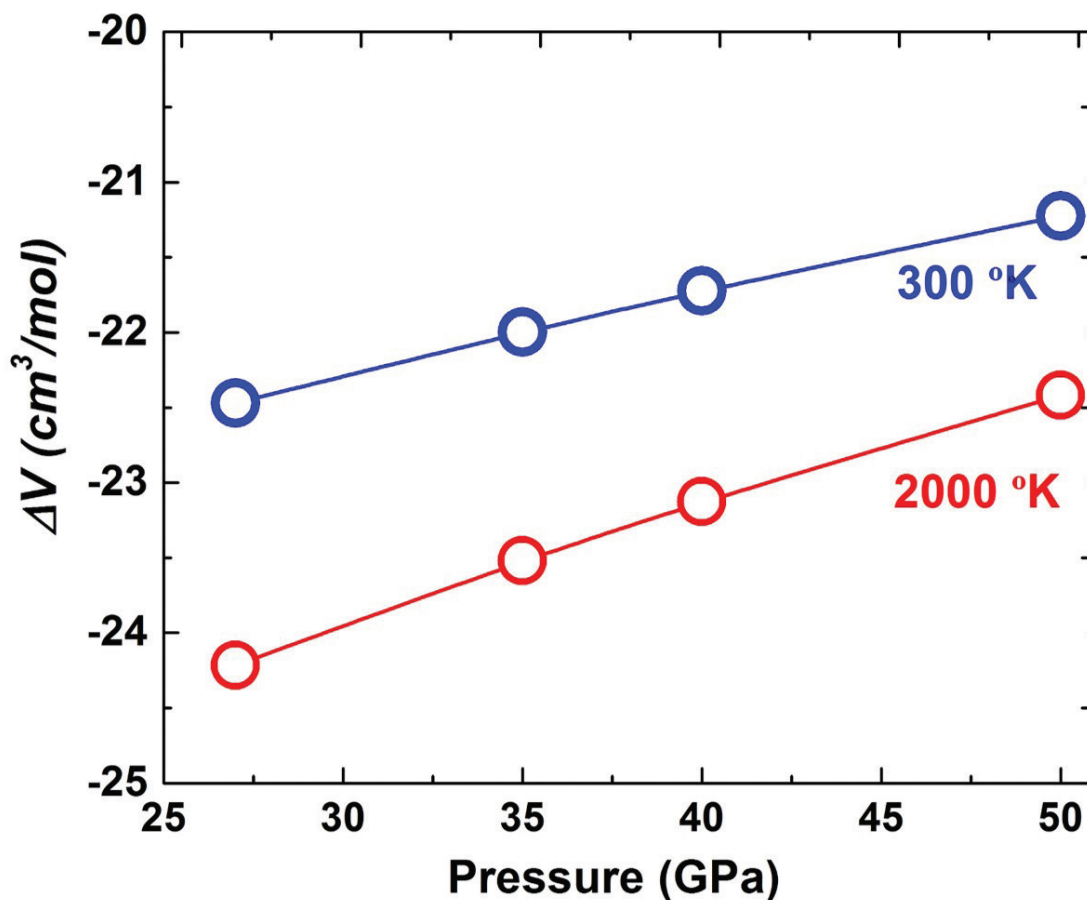


Figure S-5 The calculated molar volume change of Eq. S-2 in the text along 300 and 2000 °K, respectively.

Supplementary Information References

- AKAOGI, M., ITO, E. (1999) Calorimetric study on majorite–perovskite transition in the system $\text{Mg}_4\text{Si}_4\text{O}_{12}$ – $\text{Mg}_3\text{Al}_2\text{Si}_3\text{O}_{12}$: transition boundaries with positive pressure–temperature slopes. *Physics of the Earth and Planetary Interiors* 114, 129–140.
- FUNAMORI, N., YAGI, T., UTSUMI, W., KONDO, T., UCHIDA, T., FUNAMORI, M. (1996) Thermoelastic properties of MgSiO_3 perovskite determined by in situ X ray observations up to 30 GPa and 2000 K. *Journal of Geophysical Research* 101, 8257–8269.
- IRIFUNE, T., KOIZUMI, T., ANDO, J. (1996) An experimental study of the garnet–perovskite transformation in the system MgSiO_3 – $\text{Mg}_3\text{Al}_2\text{Si}_3\text{O}_{12}$. *Physics of the Earth and Planetary Interiors* 96, 147–157.
- ITO, E., MATSUI, Y. (1978) Synthesis and crystal–chemical characterization of MgSiO_3 perovskite. *Earth and Planetary Science Letters* 38, 443–450.
- KATSURA, T., YOKOSHI, S., KAWABE, K., SHATSKIY, A., MANTHILAKE, M., ZHAI, S. M., FUKUI, H., HEGODA, H., YOSHINO, T., YAMAZAKI, D., MATSUZAKI, T., YONEDA, A., ITO, E., SUGITA, M., TOMIOKA, N., HAGIYA, K., NOZAWA, A., FUNAKOSHI, K. (2009) P–V–T relations of MgSiO_3 perovskite determined by in situ X-ray diffraction using a large-volume high-pressure apparatus. *Geophysical Research Letters* 36, L01305.
- KOJITANI, H., KATSURA, T., AKAOGI, M. (2007) Aluminum substitution mechanisms in perovskite-type MgSiO_3 : An investigation by Rietveld analysis. *Physics and Chemistry of Minerals* 34, 257–267.
- KOJITANI, H., ISHII, T., AKAOGI, M. (2012) Thermodynamic investigation of phase equilibrium boundary between calcium ferrite-type MgAl_2O_4 and $\text{MgO} + \text{Al}_2\text{O}_3$. *Physics of the Earth and Planetary Interiors* 212–213, 100–105.
- KONO, Y., IRIFUNE, T., HIGO, Y., INOUE, T., BARNHOORN, A. (2010) PVT relation of MgO derived by simultaneous elastic wave velocity and in situ X-ray measurements: A new pressure scale for the mantle transition region. *Physics of the Earth and Planetary Interiors* 183, 196–211.
- KUBO, A., AKAOGI, M. (2000) Post-garnet transitions in the system $\text{Mg}_4\text{Si}_4\text{O}_{12}$ – $\text{Mg}_3\text{Al}_2\text{Si}_3\text{O}_{12}$ up to 28 GPa: phase relations of garnet, ilmenite and perovskite. *Physics of the Earth and Planetary Interiors* 121, 85–102.
- LIU, Z.D., IRIFUNE, T., NISHI, M., TANGE, Y., ARIMOTO, T., SHINMEI, T. (2016) Phase relations in the system MgSiO_3 – Al_2O_3 up to 52 GPa and 2000 K. *Physics of the Earth and Planetary Interiors* 257, 18–27.
- NAVROTSKY, A., SCHOENITZ, M., KOJITANI, H., XU, H., ZHANG, J., WEIDNER, D.J., JEANLOZ, R. (2003) Aluminum in magnesium silicate perovskite: Formation, structure, and energetics of magnesium-rich defect solid solutions. *Journal of Geophysical Research* 108, 2330.
- TANGE, Y., KUWAYAMA, Y., IRIFUNE, T., FUNAKOSHI, K.-I., OHISHI, Y. (2012) P–V–T equation of state of MgSiO_3 perovskite based on the MgO pressure scale: A comprehensive reference for mineralogy of the lower mantle. *Journal of Geophysical Research* 117, B06201.
- WALTER, M., KUBO, A., YOSHINO, T., BRODHOLT, J., KOGA, K.T., OHISHI, Y. (2004) Phase relations and equation-of-state of aluminous Mg–silicate perovskite and implications for Earth’s lower mantle. *Earth and Planetary Science Letters* 222, 501–516.
- WALTER, M., TRONNES, R.G., ARMSTRONG, L.S., LORD, O., CALDWELL, W.A., CLARK, A.M. (2006) Subsolidus phase relations and perovskite compressibility in the system MgO – $\text{AlO}_{1.5}$ – SiO_2 with implications for Earth’s lower mantle. *Earth and Planetary Science Letters* 248, 77–89.
- WENG, K., MAO, H.K., BELL, P.M. (1981) Lattice parameters of the perovskite phase in the system MgSiO_3 – CaSiO_3 – Al_2O_3 . *Carnegie Institute Washington, Year Book* 81, 273–277.
- YAGI, T., OKABE, K., NISHIYAMA, N., KUBO, A., KIKEGAWA, T. (2004) Complicated effects of aluminum on the compressibility of silicate perovskite. *Physics of the Earth and Planetary Interiors* 143–144, 81–89.
- ZHANG, J., WEIDNER, D.J. (1999) Thermal equation of state of aluminum–enriched silicate perovskite. *Science* 284, 782–784.

